

# Prospects for Studies of Stellar Evolution and Stellar Death in the *JWST* Era

Michael J. Barlow

Department of Physics & Astronomy,  
University College London,  
Gower Street, London WC1E 6BT, U.K.

**Abstract.** I review the prospects for studies of the advanced evolutionary stages of low-, intermediate- and high-mass stars by the *JWST* and concurrent facilities, with particular emphasis on how they may help elucidate the dominant contributors to the interstellar dust component of galaxies. Observations extending from the mid-infrared to the submillimeter can help quantify the heavy element and dust species inputs to galaxies from AGB stars. *JWST*'s MIRI mid-infrared instrument will be so sensitive that observations of the dust emission from individual intergalactic AGB stars and planetary nebulae in the Virgo Cluster will be feasible. The *Herschel Space Observatory* will enable the last largely unexplored spectral region, from the far-IR to the submm, to be surveyed for new lines and dust features, while *SOFIA* will cover the wavelength gap between *JWST* and *Herschel*, a spectral region containing important fine structure lines, together with key water-ice and crystalline silicate bands. *Spitzer* has significantly increased the number of Type II supernovae that have been surveyed for early epoch dust formation but reliable quantification of the dust contributions from massive star supernovae of Type II, Type Ib and Type Ic to low- and high-redshift galaxies should come from *JWST* MIRI observations, which will be able to probe a volume over 1000 times larger than *Spitzer*.

## 1 Introduction

The bulk of the heavy element enrichment of the interstellar media of galaxies is a result of mass loss during the final evolutionary stages of stars, yet these final stages are currently the least well understood parts of their lives. This is because (a) relatively short evolutionary timescales often lead to comparatively small numbers of objects in different advanced evolutionary stages; (b) strong mass loss with dust formation during some late phases can lead to self-obscuration at optical wavelengths, requiring infrared surveys for their detection; (c) the mass loss process itself can have a complex dependence on pulsational properties, metallicity and the physics of dust formation. For low and intermediate mass stars ( $\leq 8 M_{\odot}$ ), strong mass loss during the asymptotic giant branch (AGB) phase (Iben & Renzini 1983) exposes the dredged-up products of nucleosynthesis (nitrogen from CNO-cycle H-shell burning and carbon from helium-shell burning). For higher mass stars, mass loss stripping eventually exposes the products of H- and He-burning. During the late stages of massive stars these products can dominate their spectra, as luminous blue variables (LBVs) or as WN, WC or WO Wolf-Rayet (WR) stars.

Current or planned optical and infrared surveys of the Milky Way Galaxy (MWG) and of other Local Group galaxies will yield much larger samples of single and binary stars in the various brief evolutionary phases that occur near the end-points of their lives. Ground-based optical surveys include the nearly complete INT Photometric H $\alpha$  Survey of the northern galactic plane (IPHAS; Drew et al. 2005) and the complementary VST Photometric H $\alpha$  Survey (VPHAS+) of the southern galactic plane that will begin in 2009, while ground-based near-IR surveys include the UKIRT Infrared Deep Sky Survey (UKIDSS; Lawrence et al. 2007) in the north, and the VISTA sky surveys in the south. From space, we have the recent *Spitzer* GLIMPSE (Benjamin et al. 2003) and MIPS GAL (Carey et al. 2005) mid-IR surveys of the MWG between  $l = \pm 60^\circ$ , which will be joined by the *Herschel* 70-500  $\mu\text{m}$  Hi-GAL Survey of the same MWG regions, while the *Spitzer* SAGE survey (Meixner et al. 2006) and the *Herschel* Heritage survey will map the contents of the lower metallicity LMC and SMC dwarf galaxies from 3.6 to 500  $\mu\text{m}$ . These surveys will enable many stars in different advanced evolutionary stages to be identified, from their characteristic optical/IR spectral energy distributions (SEDs).

The *JWST* is an infrared observatory and a significant number of its concurrent facilities will operate at infrared and submillimeter wavelengths. The gaseous component of mass loss outflows can be studied in detail at these wavelengths using high resolution spectrometers. In addition, towards the end-points of their evolution many stars become extremely luminous at infrared wavelengths due to re-emission by dust particles formed in their outflows. This dust emission can be used as a tool for studying stellar populations, for studying the mass loss process and its history and for investigating the effects of stellar evolution on the enrichment of galaxies. Carbon and silicate dust particles are thought to be ubiquitous throughout our Galaxy but where are these particles formed? Evolved stars (AGB stars, M supergiants, WR stars, supernovae, etc.) are known to be significant sources of dust particles but what are the dominant sources of dust in our own and other galaxies? Tielens, Waters and Bernatowicz (2005) summarised current estimates for the gas and dust inputs to the ISM of our galaxy from various classes of evolved stars; their review pinpoints the fact that the integrated contributions by some of these stellar types have large uncertainties at present.

As a result of ongoing measurements of mass loss rates by the *Spitzer* SAGE Survey, the dominant stellar dust contributors to the metal-poor LMC and SMC dwarf galaxies, at known distances, will soon be known. For the much more massive Milky Way Galaxy, the optical and IR surveys discussed above will lead to much larger samples of hitherto rare evolved star types. Once accurate parallaxes become available for one billion MWG stars down to 20th magnitude from ESA's GAIA Mission (2012-20), then we will have reliable distances, population numbers and mass loss rates for a wide range of evolutionary types, allowing accurate gas and dust enrichment rates for the MWG to be established. In this review I will focus on future observations by the *JWST* and other new facilities of low-, intermediate- and high-mass stars in the advanced evolutionary phases that are likely to provide the dominant contributions to the gas and dust enrichment of galaxies.

## 2 AGB stars, post-AGB objects and planetary nebulae

### 2.1 The infrared spectra of evolved stars

Figure 1 illustrates the mid-infrared spectra of eight oxygen-rich stars that are at different stages in their evolution up the AGB (Sylvester et al. 1999).

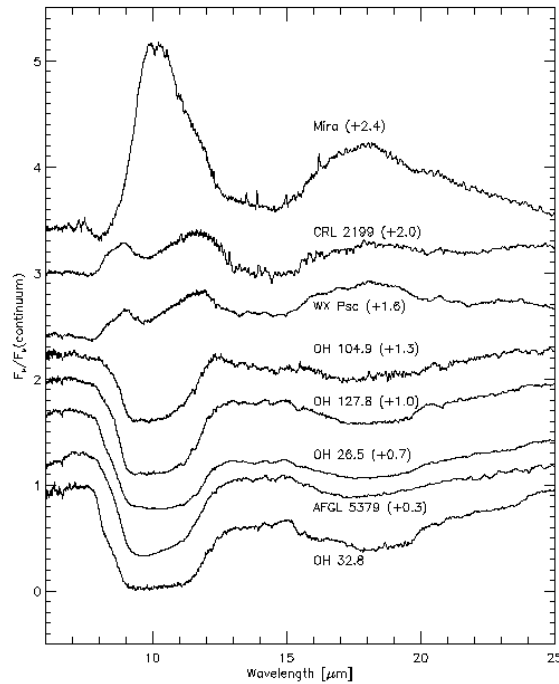


**Fig. 1.** The 6-25- $\mu\text{m}$  *ISO* SWS spectra of eight oxygen-rich AGB stars, in order of increasing mass loss rate, from top to bottom. The broad amorphous silicate features at 9.7  $\mu\text{m}$  and 18  $\mu\text{m}$  are increasingly self-absorbed with increasing mass loss rate (from Sylvester et al. 1999).

Mira (Omicron Ceti) exhibits pure emission silicate bands at 10 and 18  $\mu\text{m}$ , while CRL 2199 and WX Psc (=IRC+10011) show self-absorbed emission features and the remaining five sources show absorption features. This sequence is interpreted as one of increasing mass loss rate and increasing circumstellar self-absorption. Although the silicate-absorption objects are more luminous, the time spent at such high luminosities and mass loss rates is much shorter than the time spent lower down the AGB. The mid-IR spectra of elliptical galaxies show 10- $\mu\text{m}$  silicate features in emission (Bregman, Temi & Bregman 2006), interpreted as resulting from the combined spectra of many AGB stars having silicate emission features.



**Fig. 2.** *HST* WFPC2 F656N image of the central parts of NGC 6302, showing the obscured region (top right) attributed to an edge-on dust disk that is collimating the bipolar outflow geometry. See Matsuura et al. (2005).

For the objects shown in Fig. 1, Sylvester et al. (1999) found that after division by a smooth continuum fit, a number of sharp features were evident longwards of  $20\ \mu\text{m}$  that corresponded very well to crystalline silicate emission features that had previously been discovered in the *ISO* spectra of several classes of objects, including comets, very young stars and very evolved objects. An example of the latter is NGC 6302, a likely descendant of an extreme OH/IR star. It has a massive edge-on dust disk which completely obscures the central star, whose effective temperature is estimated from photoionization modelling to exceed 200,000 K. An *HST* image of NGC 6302 is shown in Figure 2. Its *ISO* spectrum (Figures 3 and 4) exhibits many sharp crystalline silicate emission features, as well as features due to other species, such as crystalline water ice.

The crystalline particles in NGC 6302 and other sources are thought to have been produced by the annealing of amorphous grains following upward temperature excursions. The peak wavelengths and widths of some of the features have been found to be good indicators of the temperature of the emitting particles. Figure 5 (left panel) shows laboratory spectra of the  $69\text{-}\mu\text{m}$  band of forsterite (crystalline olivine), obtained at three different temperatures (Bowey et al. 2002). As the temperature changes from 295 K to 3.5 K, the peak wavelength of the band moves

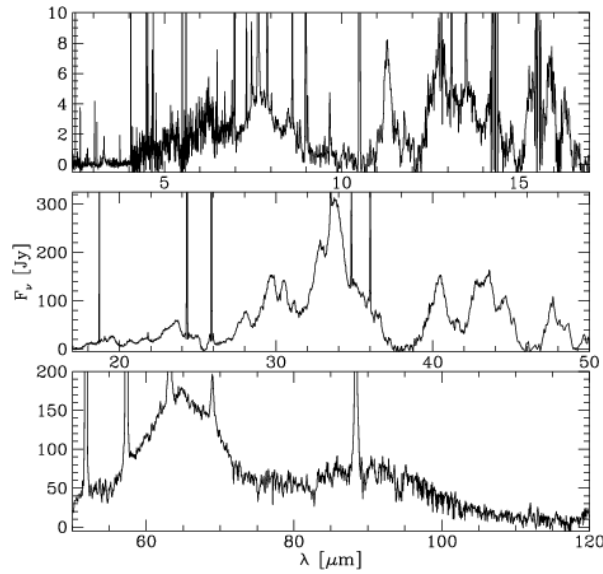


**Fig. 3.** The continuum-subtracted *ISO* SWS+LWS spectrum of the extreme bipolar planetary nebula NGC 6302, which has a massive edge-on dust disk, illustrating the presence of PAH features (top panel), as well as many crystalline silicate and water-ice features (bottom two panels). From Molster et al. (2001).

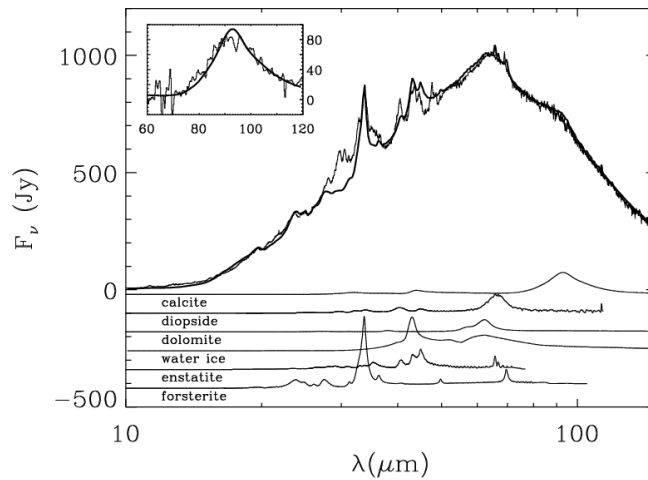


**Fig. 4.** A multi-component continuum and dust feature fit to the *ISO* far-infrared spectrum of NGC 6302 (Kemper et al. 2002). *JWST*-MIRI stops at 28  $\mu\text{m}$ . *Herschel*-PACS starts at 57  $\mu\text{m}$ . In between, there are many crystalline silicate bands, plus the crucial 44- $\mu\text{m}$  crystalline ice band and the [O III] 52- $\mu\text{m}$  line. In the next ten years, only *SOFIA* will be able to observe the 28-57- $\mu\text{m}$  wavelength range.

shortwards by nearly a micron, while the FWHM of the feature becomes narrower. The temperature derived from the peak wavelength of the 69- $\mu\text{m}$  forsterite band (Fig. 5; right panel) is well-correlated with the continuum dust temperature and thus is an excellent dust thermometer that can be used by *Herschel*-PACS and by *SOFIA* for studies of post-MS and pre-MS objects.

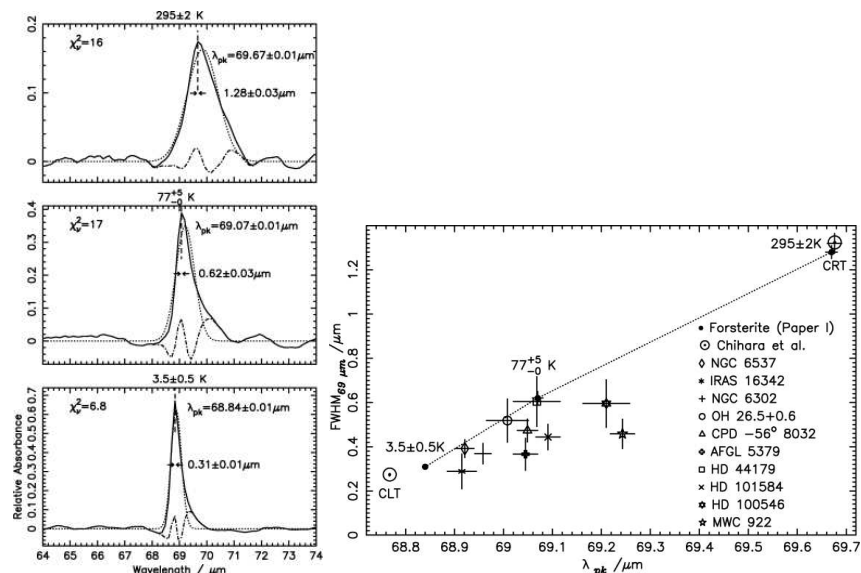


**Fig. 5.** Left: Laboratory measurements of the 69- $\mu\text{m}$  forsterite band FWHM vs. peak wavelength, for three different temperatures. Right: The FWHM versus observed peak wavelength of the 69- $\mu\text{m}$  feature for ten astronomical sources (Bowey et al. 2002).

As well as exhibiting strong crystalline silicate emission features longwards of 20  $\mu\text{m}$ , NGC 6302 also exhibits a number of emission bands in the 5-15  $\mu\text{m}$  region of its spectrum that are usually attributed to C-rich PAH particles (Figure 3, panel 1). This ‘dual dust chemistry’ phenomenon has also been encountered in the infrared spectra of a number of other post-AGB objects and planetary nebulae, particularly objects having late WC-type central stars (Cohen et al. 2002). An archetypal example of the dual dust chemistry phenomenon is the Red Rectangle bipolar nebula around the post-AGB star HD 44179 (Figure 6). Longwards of 20  $\mu\text{m}$ , its spectrum is dominated by strong crystalline silicate emission features, whereas shortwards of 15  $\mu\text{m}$  it is dominated by strong PAH emission bands. The current most favoured interpretation of dual dust chemistry sources is that the crystalline silicates reside in a cool shielded dust disk around a binary system, having been captured there following an earlier phase of AGB mass loss; later on, the AGB star evolved from an O-rich to a C-rich chemistry, following several episodes of the 3rd dredge-up, with

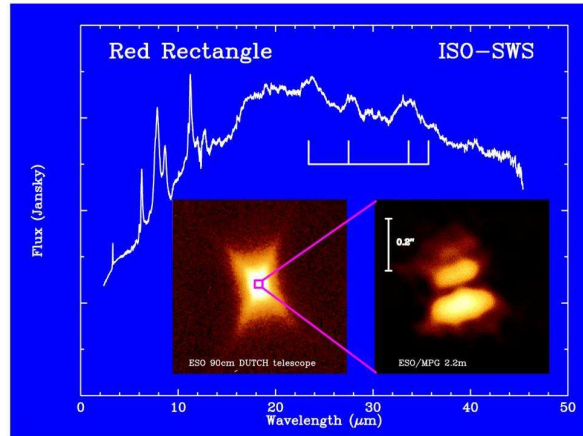


**Fig. 6.** The *ISO* SWS 2.4–45- $\mu\text{m}$  spectrum of HD 44179, the Red Rectangle, illustrating its strong PAH emission features shortwards of 15  $\mu\text{m}$  and its prominent crystalline silicate features longwards of 20  $\mu\text{m}$ . The insets show (left) a ground-based optical image of the Red Rectangle, and (right) an interferometric optical image of the central region, showing a dark dust lane cutting across the center. Figure courtesy of Frank Molster and Rens Waters

newly produced C-rich particles being channeled into polar outflows by the O-rich dust disk.

AFGL 618 and AFGL 2688 are Galactic carbon-rich bipolar post-AGB objects which, unlike the Red Rectangle, do not exhibit dual dust chemistries, with only carbon-rich molecular or dust features having been detected in their spectra. Cernicharo et al. (2001) identified absorption features due to benzene and several other complex hydrocarbon molecules in the *ISO* SWS spectrum of AFGL 618, while Bernard-Salas et al. (2006) have detected the same absorption features in an  $R = 600$  *Spitzer* IRS spectrum of SMP LMC11 (Figure 7), an LMC object that has been classified in the past as a planetary nebula, but whose IR spectrum and *HST* image (Fig. 7) indicate it as likely to be transiting between the post-AGB and ionized PN phases. As can be seen in Fig. 7, the 14.85- $\mu\text{m}$  benzene absorption feature is even stronger in the spectrum of SMP LMC11 than in the spectrum of AFGL 618.

## 2.2 Potential JWST studies of extragalactic evolved stars and planetary nebulae

SMP LMC11 is an example of a potential target for higher spectral resolution infrared spectroscopy by *SOFIA* (apart from the 13.5–16.5  $\mu\text{m}$  region, which is inaccessible even from airborne altitudes) or by *JWST*-MIRI. However, it is worth bearing in mind that even at the distance of the LMC, SMP LMC11, with a peak flux of  $\sim 0.5$  Jy (Fig. 7), will only just be observable using MIRI's  $R = 3000$  integral field spectroscopy mode, given the expected 0.5 Jy saturation limit of this

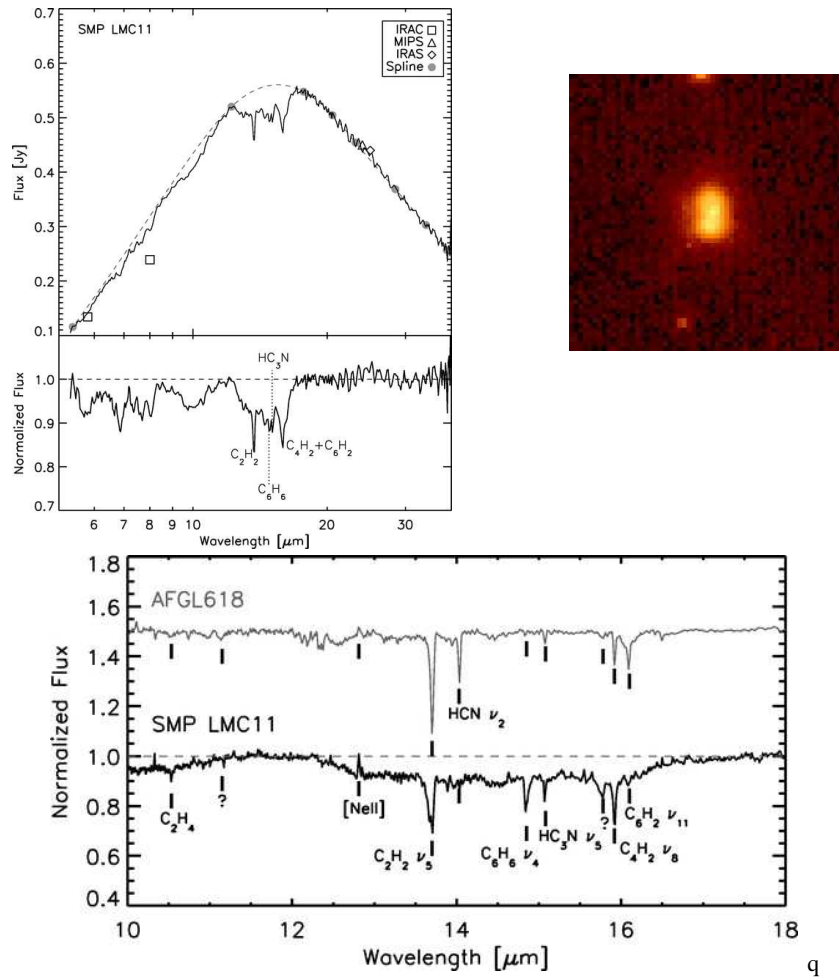


**Fig. 7.** Top-left: The *Spitzer*-IRS spectrum of the proto-planetary nebula SMP LMC11 (Bernard-Salas et al. 2006) showing both fluxed and normalized versions, with several hydrocarbon absorption features identified. Bottom: Normalized 10-18- $\mu\text{m}$  spectra of AFGL 618 (Cernicharo et al. 2001) and SMP LMC11 (Bernard-Salas et al. 2006), showing absorption features due to benzene and other complex hydrocarbons. Top-right: *HST* V-band image of SMP LMC11, from Shaw et al. (2006), showing its bipolar structure.

mode. This starkly illustrates the huge sensitivity gains that MIRI will confer relative to previous mid-infrared instrumentation. Photometric studies with MIRI of AGB stars and post-AGB nebulae will generally only be feasible for targets lying at much greater distances than the Magellanic Clouds.

Using *JWST*'s MIRI in its  $1.3' \times 1.7'$  imaging mode, SMP LMC11 would be detectable at  $10\sigma$  in  $10^4$  sec out to a distance of 18 Mpc at  $18 \mu\text{m}$ ; out to a distance of 38 Mpc at  $10 \mu\text{m}$ ; and out to a distance of 47 Mpc at  $7.5 \mu\text{m}$ . Objects discovered via imaging photometry could be followed up from 5-10  $\mu\text{m}$  with MIRI's long-slit R = 100 spectrometer. SMP LMC11 would yield  $10\sigma$  per spectral resolution element in  $10^4$  sec at a distance of 14.5 Mpc. These numbers indicate that in the above modes MIRI will be comfortably capable of studying similar objects out to the Virgo Cluster ( $D \sim 14$  Mpc) and beyond.

**A case study: the intergalactic stellar population of the Virgo Cluster** In recent years planetary nebulae have become important probes of extragalactic stellar systems. Up to 10% of the total luminosity of a planetary nebula,  $\sim 500 L_{\odot}$ , can be emitted in the dominant cooling line, [O III]  $\lambda 5007$ . This, coupled with the narrowness of the line ( $\sim 15\text{-}25 \text{ km s}^{-1}$ ), makes it extremely easy to detect PNe in external galaxies using a narrow-band filter tuned to the galaxy redshift.

Arnaboldi et al. (1996) measured velocities for 19 PNe in the outer regions of the giant elliptical galaxy NGC 4406, in the southern Virgo extension region. Although this galaxy has a peculiar radial velocity of  $-227 \text{ km s}^{-1}$ , three of the PNe had velocities close to  $1400 \text{ km s}^{-1}$ , the mean radial velocity of the Virgo cluster. It was concluded that they were intracluster PNe. Theuns & Warren (1997) discovered ten PN candidates in the Fornax cluster, in fields well away from any Fornax galaxy - consistent with tidal stripping of cluster galaxies. They estimated that intracluster stars could account for up to 40% of all the stars in the Fornax cluster. Mendez et al. (1997) surveyed a  $50 \text{ arcmin}^2$  area near the centre of the Virgo cluster, detecting 11 PN candidates. From this, they estimated a total stellar mass of about  $4 \times 10^9 M_{\odot}$  in their survey area and that such a population could account for up to 50% of the total stellar mass in the Virgo cluster.

Follow-up observations have confirmed large numbers of intergalactic PN candidates in Virgo. However, they represent a tiny tip of a very large iceberg. How to sample more of the iceberg? The discussion above of *JWST* MIRI capabilities indicates that mid-infrared observations of dust-emitting AGB stars and planetary nebulae located in intergalactic regions of the Virgo Cluster are feasible.

Figure 8 shows the *Spitzer* mid-infrared spectra of two LMC planetary nebulae. The fluxes measured for the SiC-emitting nebula SMP LMC8 indicate that in  $10^4$  sec MIRI imaging would yield  $10\sigma$  detections for a distance of  $D = 19$  Mpc with the 7.7- and 11.3- $\mu\text{m}$  filters and for a distance of 13 Mpc with the 18- $\mu\text{m}$  filter. For the strongly PAH-emitting PN SMP LMC36, in  $10^4$  sec MIRI imaging would yield a  $10\sigma$  detection for a distance of 44 Mpc with the 7.7- $\mu\text{m}$  filter and for a distance of 23 Mpc with the 11.3- $\mu\text{m}$  filter. The carbon star MSX SMC 159, whose *Spitzer* IRS spectrum is shown in Figure 9 (from Sloan et al. 2006), would yield  $10\sigma$  detec-

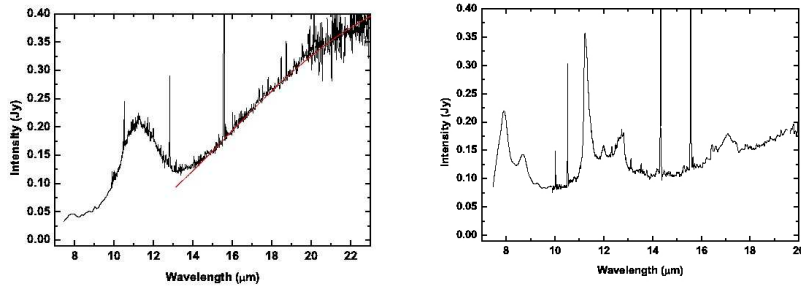


**Fig. 8.** *Spitzer*-IRS spectra of (left) SMP LMC8, showing a strong SiC 11.2- $\mu\text{m}$  emission feature and (right) SMP LMC36, showing very strong PAH emission bands. Both planetary nebulae also exhibit narrow fine structure ionic emission lines in their spectra.

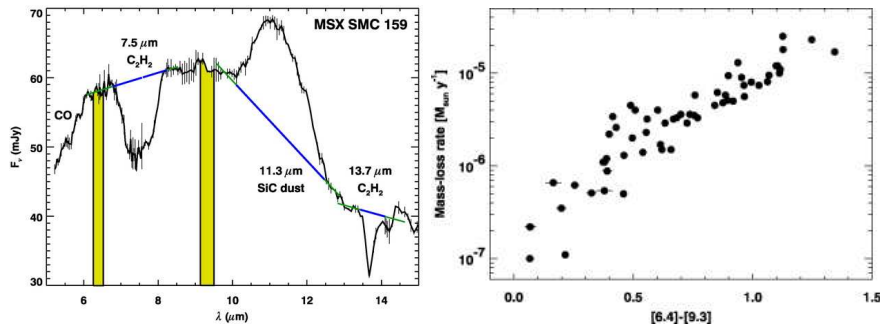


**Fig. 9.** Left: the *Spitzer* IRS spectrum of the carbon star MSX SMC 159, illustrating the 11.2- $\mu\text{m}$  SiC dust emission feature, as well as several important molecular absorption features and the narrow ‘continuum’ regions defined at 6.4  $\mu\text{m}$  and 9.3  $\mu\text{m}$  by Sloan et al. (2006). Right: a plot from Groenewegen et al. (2007) of the correlation between the *Spitzer* [6.4]-[9.3] colors of SMC carbon stars and their derived mass loss rates.

tions in  $10^4$  sec with MIRI out to a distance of  $D = 29$  Mpc with the 5.6- $\mu\text{m}$  filter, to 23 Mpc with the 7.7- $\mu\text{m}$  filter and to 12 Mpc with the 11.3- $\mu\text{m}$  filter. Similar detection limits apply for oxygen-rich AGB stars. As shown by Groenewegen et al. (2007; see Fig. 9), mid-infrared colour indices can be used to estimate mass loss rates and thereby mass inputs from stellar populations hosting AGB stars.

As well as MIRI, the other *JWST* instruments will also be useful for such studies, e.g. with the *JWST* Tunable Filter Imager ( $R = 100$ ), a carbon star similar to MSX SMC 159 would give  $10\sigma$  per resolution element in  $10^4$  sec for distances out to  $D = 24$ -29 Mpc, for wavelengths from 2 – 4  $\mu\text{m}$ . There are at least 20-30 AGB stars for every PN, so there should be many detectable AGB stars in Virgo Cluster fields, allowing the total stellar population to be determined, as well as their gas and dust mass inputs into the intracluster medium.

### 2.3 Exploring new wavelength regions at high spectral resolution

The 200-650  $\mu\text{m}$  range is the last largely unexplored region of the astronomical spectrum. Many spectral lines and features were observed for the first time in the 45-200  $\mu\text{m}$  region by *ISO*'s Long Wavelength Spectrometer, e.g. Figure 10 shows the LWS spectra of the oxygen-rich M supergiant VY CMa and the carbon star IRC+10<sup>0</sup>216. Similar numbers of new lines and features can be expected to be found in the 200-650  $\mu\text{m}$  spectral region. The HIFI, PACS and SPIRE spectrometers on-board ESA's *Herschel Space Observatory* will observe a large number of targets in this wavelength range. HIFI is capable of obtaining complete spectral scans from 157-625  $\mu\text{m}$  at a resolving power of  $R = 10^6$  for a range of archetypal O-rich and C-rich sources, which would allow an unprecedented line inventory to be built up. By measuring line fluxes and profiles with high spectral resolution, HIFI and later ALMA will be able to probe the dynamics of stellar wind outflows and to use a wide range of atomic and molecular species to study the wind chemistry and thermal structure as a function of distance from the central source, with the strong cooling lines of CO, HCN and H<sub>2</sub>O being particularly well-suited to probing the thermal and density structures of stellar winds. The superb sensitivity of ALMA will allow detailed studies to be made of objects located throughout the Milky Way and in the Magellanic Clouds. In addition, its high angular resolution will make it very well-suited to probe the dynamical and physical conditions in the complex nebulae found around some AGB stars, post-AGB objects and planetary nebulae.

The *Herschel* SPIRE FTS will obtain spectra at up to  $R = 1000$  for a large number of O-rich and C-rich sources from 200-650  $\mu\text{m}$ , searching particularly for new dust features that may be present. These features may also occur in the spectra of star forming regions and galaxies, but the best place to isolate and identify them is in the spectra of objects with known chemistries, around which they have formed. In addition, the continuum spectral properties of different dust species, particularly their emissivity laws, have yet to be fully characterised in this spectral region.

### 2.4 The 'missing mass' problem for intermediate mass stars

An 'average' planetary nebula has a central star mass of  $\sim 0.6 M_{\odot}$  and a nebular mass of  $\sim 0.3 M_{\odot}$ . Population modelling predicts a typical main sequence progenitor mass of  $1.3 M_{\odot}$ , so about  $0.4 M_{\odot}$  appears to have been lost during earlier stages of evolution. A much greater discrepancy exists for intermediate mass progenitors. Populations of white dwarfs have been found in open clusters which have main sequence turn-off masses of 6-8  $M_{\odot}$  (e.g. in NGC 2516; see Weidemann 2000). So, 5 – 7  $M_{\odot}$  must have been lost in order to allow such stars to get below the Chandrasekhar limit, yet the most massive PNe (e.g. NGC 6302, NGC 7027) contain no more than 2  $M_{\odot}$  of nebular material. So when was the rest of the mass lost (and how do stars that develop degenerate cores know about the Chandrasekhar limit?) There is an obvious need for a comprehensive survey of the mass loss histories of evolved stars.

The most sensitive method to search for ejected material around evolved stars is to image the FIR/submm emission from dust particles in the ejecta that are being

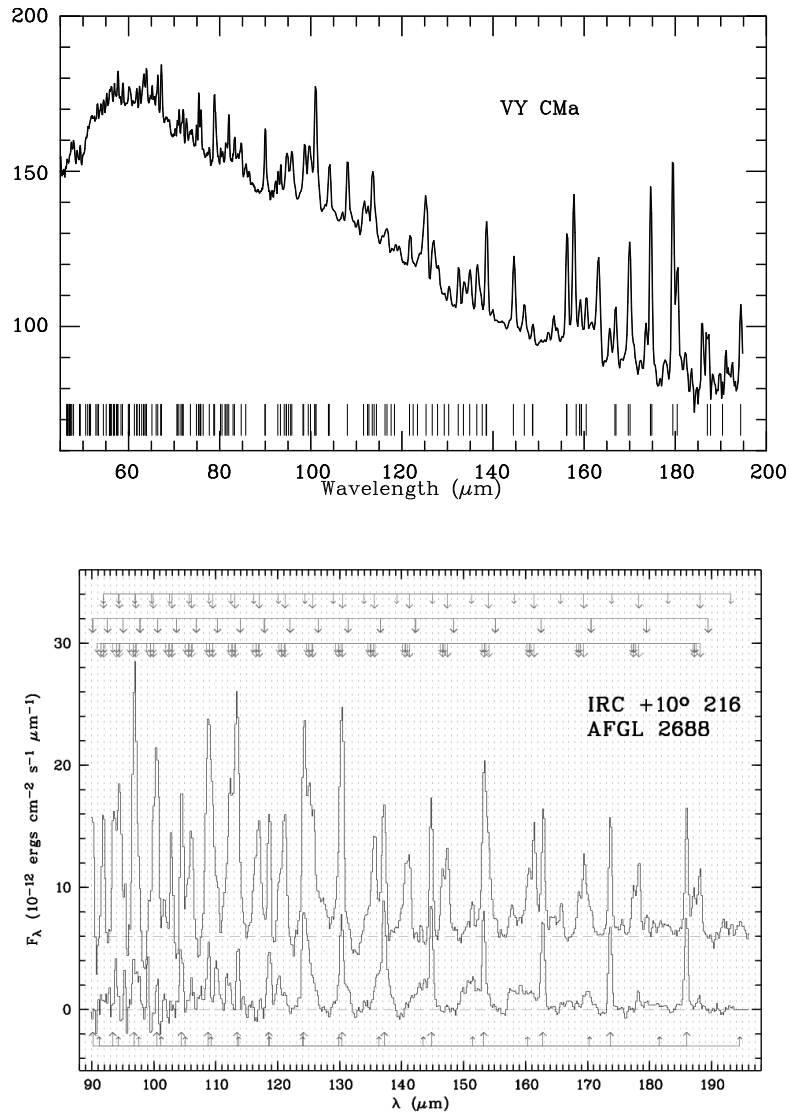


**Fig. 10.** *Top:* The 43-197  $\mu\text{m}$  *ISO* LWS spectrum of the M supergiant VY CMa. The observed flux ( $F_\lambda$ ) has been multiplied by  $\lambda^4$  to show this Rayleigh-Jeans region of the spectrum more clearly. The tick marks at the bottom indicate the wavelengths of some of the ortho- and para- $\text{H}_2\text{O}$  rotational lines in this spectral region. Over 100 water lines are detected. *Bottom:* The continuum-subtracted 90-197  $\mu\text{m}$  *ISO* LWS spectra of the carbon star IRC+10°216 (upper spectrum) and of the C-rich post-AGB object AFGL 2688 (lower spectrum). The upward pointing arrows indicate the positions of  $v=0$  and  $v=1$  rotational lines of CO. The downward pointing arrows indicate the positions of rotational lines of HCN and  $\text{H}^{13}\text{CN}$ , as well as of vibrationally excited HCN rotational lines. See Cernicharo et al. (1996) and Cox et al. (1996) for more details on the carbon-rich source spectra.

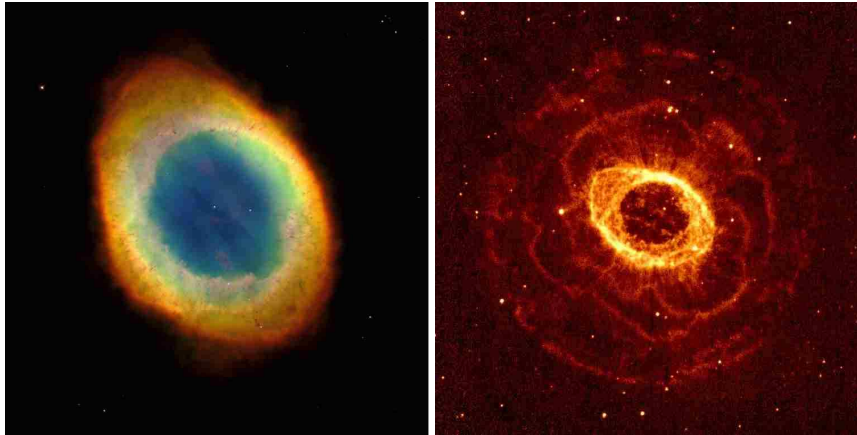


**Fig. 11.** Left: An *HST* WFPC2 publicity image of the Ring Nebula, NGC 6720, taken by combining exposures in each of three filters. Red: F658N ([N II]), green: F501N ([O III]), Blue: F469N (He II). The FoV is  $2 \times 2$  arcmin. Right: a publicity image of the Ring Nebula seen observed in the  $\text{H}_2$   $v=1-0$  S(1)  $2.122\text{-}\mu\text{m}$  line with the MPA Omega near-IR camera on the Calar Alto 3.5-m telescope. The FoV is  $5 \times 5$  arcmin. The bright inner emission corresponds to the optical nebula; the outer rosette-shaped filaments correspond to  $\text{H}_2$  emission from material that is situated well beyond the optically emitting nebula.

heated by the interstellar radiation field to temperatures of 20–30 K, peaking at far-IR wavelengths. Ionized gas can only be detected following the onset of the planetary nebula phase, while cool rarefied atomic or molecular gas can be extremely difficult to detect except in favorable circumstances (Figure 11 shows the  $\text{H}_2$ -emitting halo detected around the Ring Nebula). On the other hand, spatially extended dust emission from ejected material is much easier to detect, during any phase of evolution. Very extended dust shells have been detected around a number of AGB stars, in *IRAS* and *ISO* far-infrared images (see e.g. Izumiura et al. 1996, and references therein).

Compared to earlier facilities, the *Herschel Space Observatory* will have a greatly enhanced sensitivity to extended emission at far-infrared and submillimeter wavelengths. Following its launch in 2008/9, one of its Guaranteed Time programmes will carry out mapping observations aimed at detecting and determining the masses of extended dust shells around a wide range of evolved star classes, in order to trace their mass loss histories. Shells produced by past mass loss events over periods of up to 40,000 years are potentially detectable and can yield information on the mass loss process itself, e.g. whether it has been continuous or episodic. Multi-wavelength photometric imaging can yield fluxes, dust temperatures and dust shell masses. The PACS and SPIRE instruments will obtain scanned maps of up to  $30 \times 30$  arcmin at 70, 110, 250, 350 and  $520 \mu\text{m}$  for a large sample of targets, including AGB stars (O-rich and C-rich), post-AGB objects and PNe. High galactic latitude targets will be favoured, to minimise background confusion. High spectral resolution follow-up

observations of the [C II] 158- $\mu\text{m}$  line with *Herschel*-HIFI can provide kinematic information on extended circumstellar shells detected via imaging. Overall, these observations can lead to a better understanding and quantification of the mass loss histories of low- and intermediate-mass stars.

### 3 Dust production by massive stars

Where did the large quantities of dust detected in many high redshift galaxies originate from? Bertoldi et al. (2003) detected redshifted warm dust emission at millimeter wavelengths from three QSOs with  $z > 6$ , i.e. dust had formed less than 1 Gyr after the Big Bang. Dwek, Galliano & Jones (2008) considered the case of the ultraluminous galaxy SDSS J1148+5251, at  $z = 6.4$ . Its IR luminosity and dust mass were estimated to be  $2 \times 10^{13} L_{\odot}$  and  $2 \times 10^8 M_{\odot}$ , respectively, with its luminosity implying a current star formation rate of  $\sim 3000 M_{\odot} \text{ yr}^{-1}$ . At  $z = 6.4$ , the Universe was only 900 Myr old; if the galaxy formed at  $z = 10$ , then it is only 400 Myr old. In fact, given its estimated dynamical mass of  $5 \times 10^{10} M_{\odot}$ , its current star formation rate would give an age of only 20 Myr. An age of 20 – 400 Myr would be insufficient for AGB stars to appear - only massive stars would have had sufficient time to evolve and produce dust. Elvis, Marengo & Karovska (2002) suggested that QSO winds could reach temperatures and pressures similar to those found around cool dust-forming stars and that up to  $10^7 M_{\odot}$  of dust could be formed. Markwick-Kemper et al. (2008) observed the  $z = 0.466$  broad absorption line QSO PG 2112+059 with the *Spitzer* IRS and detected mid-IR emission features which they attributed to amorphous and crystalline formed in the quasar wind. It is not yet clear whether all dust-emitting high- $z$  galaxies possess such AGN central engines. If massive stars should turn out to be the dominant sources of dust in high- $z$  galaxies, which of their evolutionary phases is the dominant dust producer? Is it the late-type supergiant phase, the Luminous Blue Variable phase, the Wolf-Rayet phase, or the final core-collapse supernova event?

#### 3.1 Late-type Supergiants and Hypergiants

The M2 Iab supergiant  $\alpha$  Orionis, with a luminosity of  $\sim 2.5 \times 10^5 L_{\odot}$ , has been estimated to have a gas mass loss rate of  $\sim 1.5 \times 10^{-5} M_{\odot} \text{ yr}^{-1}$  (Jura & Morris 1981). More luminous late type supergiants (sometimes dubbed ‘hypergiants’) can have even higher mass loss rates and are often self-obscured by their own circumstellar dust at optical wavelengths, e.g. the red hypergiants VY CMa (Fig. 10), VX Sgr and NML Cyg. Similarly high mass loss rates can be exhibited by yellow hypergiants, e.g.  $\rho$  Cas, IRC+10 420 and HR 8752. Such objects could potentially make a very significant contribution to the dust enrichment of galaxies but currently we do not know the duration of the yellow/red hypergiant phase, nor the total population of such objects in our galaxy. Better statistics from current optical and near-IR surveys, together with distances from Gaia and more precise mass loss rate determinations using improved wind modelling techniques, should lead to a much improved

understanding of the contribution of these objects to the dust and gas evolution of galaxies.

### 3.2 Luminous Blue Variables and Wolf-Rayet stars

The ejecta nebulae around Luminous Blue Variables (LBVs) can contain large masses of dust, as in the cases of  $\eta$  Car and AG Car (though not in the case of P Cygni); the 1840's outburst of  $\eta$  Car has been estimated to have produced  $0.2 M_{\odot}$  of dust (Morris et al. 1999). The M 1-67 ejecta nebula around the WN8 Wolf-Rayet star WR124 (Fig. 12) also contains large quantities of dust and is thought to have originated from the outburst of an LBV precursor.

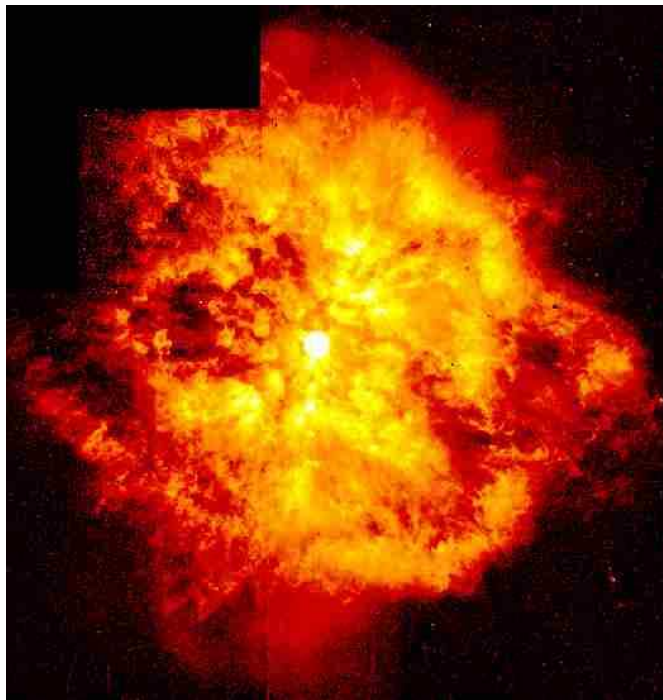


**Fig. 12.** *HST* WFPC2 F656N image of the nebula M 1-67 around the WN8 Wolf-Rayet star WR124 (=BAC 209). For further details, see Grosdidier et al. (1998).

The dust in most LBV nebulae appears to be dominated by oxygen-rich silicate grains. Massive carbon-rich WC9 Wolf-Rayet stars often show hot ( $\sim 900$  K) featureless dust emission that has been attributed to carbon grains. How does dust form in outflows from stars whose effective temperatures are in the region of 30,000 K? The answer was found by Tuthill et al. whose masked-aperture Keck imaging at

2.27- $\mu\text{m}$  revealed a rotating pinwheel plume of dust emission in the WC9+OB binary system WR104 (Fig 13). The dust appears to be formed in the compressed shock interaction region (hotspot) between the stellar winds of the WC9 primary and the OB secondary, the relative motions of the two stars creating an Archimedean spiral. Similar pinwheel structures have since been found around several more WC9 systems, including two located in the Galactic Center Quintuplet Cluster (Tuthill et al. 2006). The overall contribution of late WC-type Wolf-Rayet stars to the dust enrichment of galaxies is currently extremely uncertain. Future submm observations by ALMA can help to quantify their overall dust production rates, plus search for molecular emission from the hot-spot shocked wind compression region, while the GAIA parallax survey of the Galaxy should enable their total numbers to be more accurately estimated.

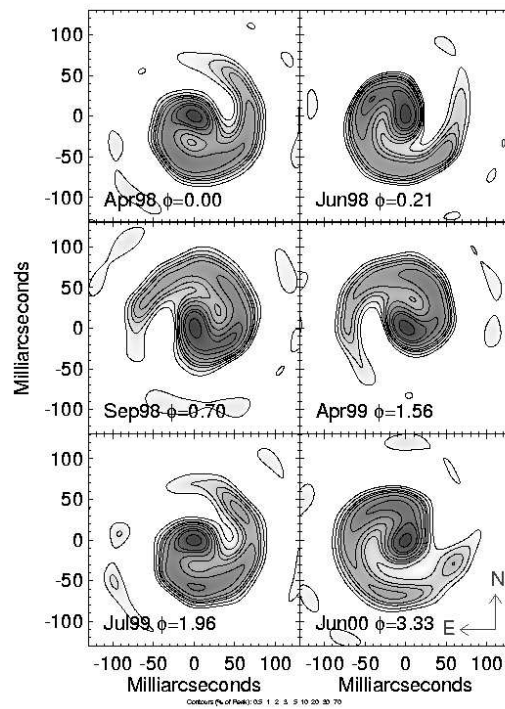


**Fig. 13.** Keck aperture-mask 2.27- $\mu\text{m}$  imaging of a rotating pinwheel plume of dust emission from the WC9+OB binary WR 104. The dust is formed in the compressed shock interaction region (hotspot) between the two stellar winds. The relative motions of the two stars creates an Archimedean spiral. From Tuthill, Monnier & Danchi (2002).

### 3.3 Core collapse supernovae

There is plenty of evidence that supernovae can synthesise dust particles that are able to survive the shock buffeting that must take place following their formation. The isotopic analysis of pre-solar meteoritic grain inclusions (those that have non-solar ratios) has found many examples that are dominated by r-process isotopes, indicating a supernova origin (e.g. Clayton, Amari & Zinner 1997). The onion-skin abundance structure of a pre-supernova massive star means that different layers of the ejecta can have  $C/O < 1$  and  $C/O > 1$ , allowing the formation of O-rich grains and C-rich grains in the respective zones. Infrared photometry and spectrophotometry of SN 1987A demonstrated the onset of thermal dust emission by day 615 (Bouchet & Danziger 1993; Wooden et al. 1993), as shown in Figure 14, the emission being attributed to newly formed dust particles in the ejecta.

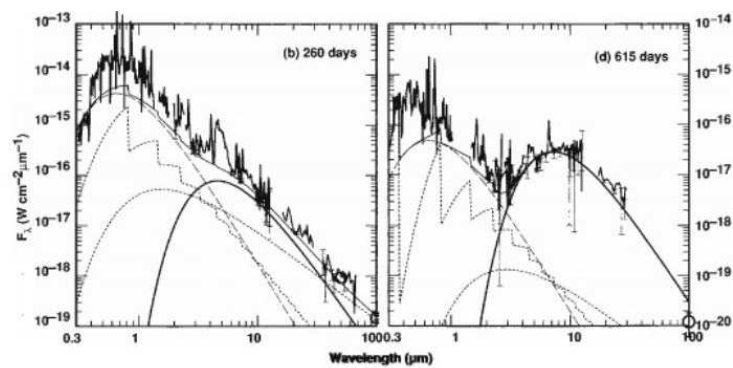


**Fig. 14.** Optical and KAO IR spectrophotometry of SN 1987A, illustrating the definite onset of thermal dust emission by day 615. From Wooden et al. (1993), who derived a lower limit of  $10^{-4} M_{\odot}$  to the mass of dust that had formed by day 775.

From dust nucleation modelling, Todini & Ferrara (2001) predicted that  $0.08\text{--}1.0 M_{\odot}$  of dust could condense in the ejecta of a typical high-redshift core collapse supernova within a few years of outburst, corresponding to a condensation efficiency for the available refractory elements of  $> 0.2$ . Similarly high condensation efficiencies appear to be required to explain the  $\sim 10^8$  solar masses of dust deduced to exist in high redshift QSOs (Morgan & Edmunds 2003; Dwek et al. 2008). However, prior to the launch of *Spitzer*, for the handful of recent core-collapse SNe for which dust formation had been inferred, the derived masses of newly formed dust were  $\leq 10^{-3} M_{\odot}$  (e.g. the examples shown in Figs. 14 and 15)

A different approach to estimating how much dust can be formed in the ejecta of a core-collapse SN was taken Dunne et al. (2003) and Morgan et al. (2003), who used SCUBA submillimeter maps to deduce that  $1\text{--}2 M_{\odot}$  of dust were present in the Cas A and Kepler supernova remnants (SNRs), both of which were less than 400

years old. However, Krause et al. (2004) argued that most of the observed submm emission observed from Cas A originated from a foreground molecular cloud that could be seen in CO maps. Deeper observations of more young SNRs across a wide wavelength range are planned in *Herschel Space Observatory* Guaranteed Time; 57 – 650  $\mu\text{m}$  PACS and SPIRE photometric and spectroscopic maps will be obtained of five galactic SNRs having ages of less than 1000 yrs (Cas A, Kepler, Tycho, Crab and 3C58)

Returning to observations of the dust formation phase itself ( $t < 1000$  days), there are currently three methods for inferring the formation of dust in supernova ejecta:

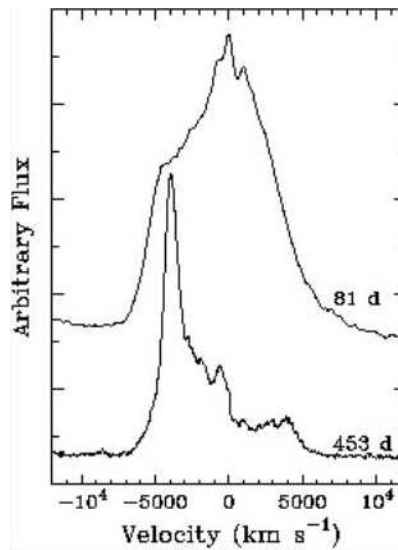


**Fig. 15.** The  $H\alpha$  line profile of SN 1998S at days 81 and 453 (Leonard et al. 2000), illustrating the loss of flux on the red side of the profile, attributed to absorption by newly formed dust preferentially removing photons from the far side of the ejecta. Pozzo et al. (2004) estimated that  $10^{-3} M_{\odot}$  of dust had formed.

1. via the detection of thermal IR emission from the newly formed dust. However, the use of this method alone can be compromised by pre-existing nearby dust (e.g. circumstellar dust), which can be heated by the supernova light flash.
2. via the detection of a dip in the SN light curve that can be attributed to extinction by newly formed dust. Pre-existing dust cannot produce such a dip.
3. via the detection of the development of a red-blue asymmetry in the SN emission line profiles, attributable to the removal by newly formed dust of some of the redshifted emission from the far side of the SN ejecta (Lucy et al. 1989; see Fig. 15).

Method (1) is normally required if dust masses are to be quantified but ideally it ought to be supported by one or both of (2) and (3).

Since the launch of the *Spitzer Space Telescope*, two teams have been conducting observing programmes to study the spectral evolution of young supernovae. Examples of the spectra of SNe less than 250 days after outburst are shown in Figure 16. The day 135 IRS spectrum of SN 2005df (Gerardy et al. 2007) shows numerous ionic fine structure lines, including lines from radioactive cobalt and nickel, whose decay is the main heating source for the ejecta. The day 214 IRS spectrum of SN 2005af (Kotak et al. 2006) is dominated by the  $\nu = 1 - 0$  band-head of gaseous SiO and is very similar to that of SN 1987A at a similar epoch.

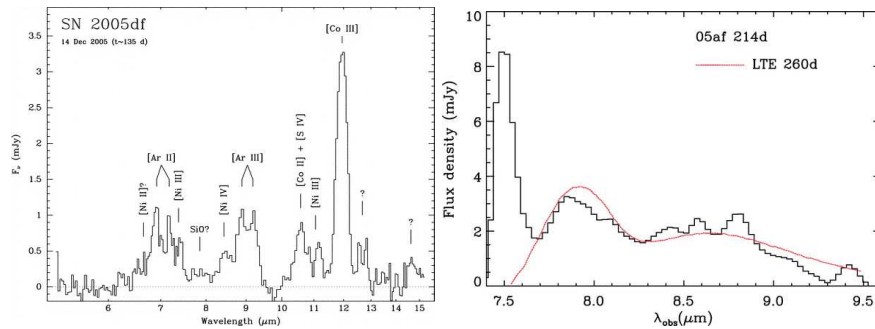


**Fig. 16.** Left: The *Spitzer* IRS spectrum of SN 2005df at day 135, showing ionic fine structure emission lines from radioactive cobalt and nickel (Gerardy et al. 2007). Right: The *Spitzer* IRS spectrum of SN 2005af at day 214, showing the  $8\text{-}\mu\text{m}$   $\nu=1-0$  bandhead of gaseous SiO (Kotak et al. 2006). By analogy to SN 1987A, this was suggested to be a precursor to dust formation.

Early in the *Spitzer* mission, dust emission from the Type IIP supernova SN 2002hh was detected in SINGS IRAC images and confirmed by higher angular resolution Gemini Michelle imaging (Barlow et al. 2005). The day 600 spectral energy distribution (SED) could be fitted by a 290 K blackbody (Fig. 17, upper), yielding a minimum emitting radius of  $R_{\min} \sim 10^{17}$  cm and a luminosity of  $L = 1.6 \times 10^7 L_{\odot}$ . A more realistic  $\lambda^{-1}$  grain emissivity gave  $R_{\min} = 5 \times 10^{17}$  cm. This was far too large for the emitting dust to have formed in the ejecta (it would have taken  $> 10$  yrs for material in the ejecta to reach this radius). It was therefore inferred that the emitting dust must have been pre-existing. All three of the model fits shown in Fig. 17 yielded total emitting dust masses in the range  $0.10 - 0.15 M_{\odot}$ . SN 2002hh is a Type IIP (plateau) supernova, whose very extended optical light curve (Welch et al. 2007) appears explicable in terms of a just-resolved light echo that has been revealed by *HST* ACS/HRC images (Sugerman 2005). Preliminary analysis indicates that the echo has occurred from a thick dust distribution that is located about 2-8 light years ( $2 - 8 \times 10^{18}$  cm) in front of the supernova.

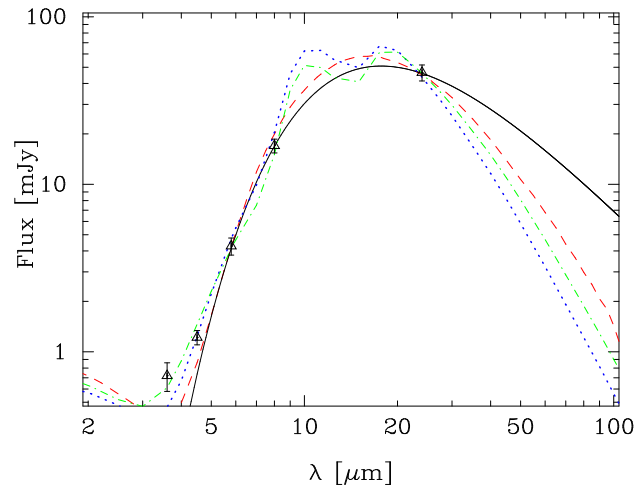


**Fig. 17.** The measured day-600 *Spitzer* 3.6–24  $\mu\text{m}$  fluxes for SN 2002hh, in NGC 6946, are shown as open triangles, with vertical bars indicating the flux uncertainties. The solid black line is a 290-K blackbody normalised to the 8.0- $\mu\text{m}$  flux point. The dashed, dotted and dash-dotted lines correspond to radiative transfer models with differing amounts of silicates and amorphous carbon; see Barlow et al. (2005).

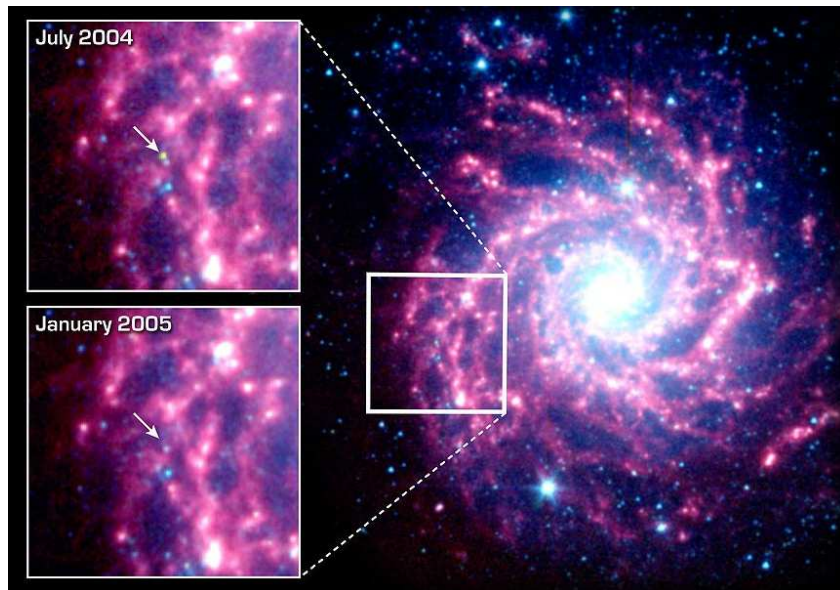


**Fig. 18.** A *Spitzer* SINGS multi-band IRAC image of NGC 628. There is a clear detection of SN 2003gd on day-499 (upper inset) relative to day-670 (lower inset). See Sugerman et al. (2006).

Sugerman et al. (2006) detected the onset of dust emission from SN 2003gd in NGC 628 (Messier 74; see Fig. 18); unlike SN 2002hh, the emitting dust was inferred to have formed inside the supernova ejecta. Between days 157 and 493 the H $\alpha$  feature developed an asymmetric profile, with a reduction in flux on the red side. This was attributed to dust forming in the ejecta preferentially extinguishing emission from receding (red-shifted) gas. There was also an increase in optical extinction after day 500, as evidenced by a dip in its light curve from that date, similar to the behaviour of SN 1987A at the same epochs. Additional extinction by dust was inferred to have occurred after day 500 for both SNe, and for SN 2003gd corresponded to 0.25 – 0.5 magnitudes in the R-band on day 500, and to 0.8 – 1.9 magnitudes on day 678.

Both smooth and clumped SN ejecta model fits to the SN 2003gd observations were presented by Sugerman et al. (2006), using a 3D Monte Carlo radiative transfer code with a mother-grid of 61<sup>3</sup> cells (the mother cells that contained clumps were resolved by a subgrid of 5<sup>3</sup> cells). To match both the optical-IR SEDs and the derived R-band extinction estimates for the SN ejecta, their day 499 data could be fitted with smoothly distributed dust having a dust mass of  $2 \times 10^{-4} M_{\odot}$ , whereas up to  $2 \times 10^{-3} M_{\odot}$  of dust could be accommodated by a clumped dust model. For day 678, their best-fit smooth dust model required  $3 \times 10^{-3} M_{\odot}$  of dust, while up to  $2 \times 10^{-2} M_{\odot}$  could be accommodated by a clumpy model, the latter implying a heavy element condensation efficiency of about 10%. The *Spitzer* observations of SN 2003gd have also been studied by Meikle et al. (2007).

**Table 1.** Thermal infrared studies of core collapse supernovae – results so far

Name	D(Mpc)	Progenitor mass, $M_{\odot}$	Dust emission?
SN 1987A	0.05	16-22	Yes
SN 1999bw	14.5	unknown	Yes, but very late
SN 2002hh	5.6	8-14	Yes, but pre-existing
SN 2003gd	9.3	6-12	Yes
SN 2004dj	3.3	12-15	Maybe; pre-existing?
SN 2004et	5.6	13-20	Yes
SN 2005cs	8.0	7-12	No

Table 1 summarises the results to date of mid-infrared searches for dust emission from young supernovae. Apart from SN 1987A, all are based on *Spitzer* observations, supplemented in two cases by Gemini North Michelle observations. Although *Spitzer* has delivered a very large increase in mid-infrared sensitivity relative to prior facilities, its distance limit for the detection of dust forming around young SNe is effectively 10-15 Mpc, corresponding to a volume within which relatively few new SNe occur each year. All of the SNe listed in Table 1 are of Type II, from progenitors with masses  $< 20 M_{\odot}$ . No Type Ib or Ic SNe, whose immediate precursors are believed to be H-deficient Wolf-Rayet stars descended from much more massive stars, have so far been close enough to be detected by *Spitzer*, although the Type Ib SN 2006jc has shown evidence for dust formation via the development of red-blue

emission line asymmetries and a transient far-red and near-IR continuum excess, interpreted by Smith, Foley & Filippenko (2008) as due to dust formation in the dense region created by the impact between the SN ejecta and slower moving material from an LBV-type eruption that was discovered two years before the supernova outburst.

For point source imaging, *Spitzer's* IRAC is  $135\times$  more sensitive at  $8\ \mu\text{m}$  than mid-IR instruments on ground-based 8-m telescopes (due to *Spitzer's* vastly lower thermal backgrounds). For point source imaging, *JWST-MIRI* is expected to be  $\sim 40\times$  more sensitive at  $8\ \mu\text{m}$  than IRAC (see [www.stsci.edu/jwst/science/sensitivity/](http://www.stsci.edu/jwst/science/sensitivity/)). In addition to these sensitivity gains, the  $8\times$  higher angular resolution of *JWST-MIRI* compared to *Spitzer-IRAC* will greatly reduce point source confusion effects in dense starfields, such as encountered when observing galaxies.

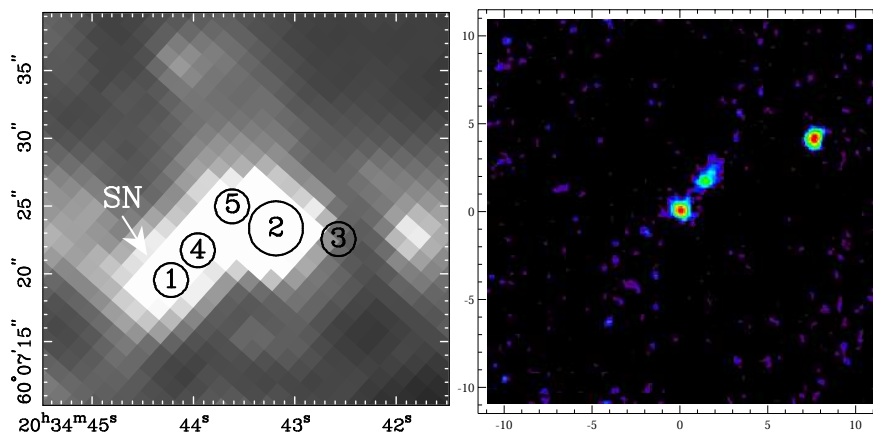


**Fig. 19.** Left: Day-590 *Spitzer* IRAC  $8\text{-}\mu\text{m}$  image of the region around SN 2002hh. With *Spitzer's* 2.4 arcsec angular resolution, five different sources are blended together. Right: the 0.3 arcsec angular resolution of this day-698 Gemini-N Michelle  $11\text{-}\mu\text{m}$  image completely resolves the sources (the SN is at the center), illustrating how in the case of crowded-field galaxy observations the high angular resolution of *JWST-MIRI* will supplement its raw sensitivity.

The angular resolution advantages of a  $>6\text{-m}$  class telescope compared to a 0.85-m telescope are illustrated in Fig. 19, where an IRAC  $8\text{-}\mu\text{m}$  image of the field of SN 2002hh, in NGC 6946, is compared to a  $8\times$  higher resolution Gemini Michelle  $11\text{-}\mu\text{m}$  image of the same field. The five sources that are blended together in the IRAC image are completely resolved from each other in the Gemini image. *MIRI's* much greater sensitivity and angular resolution should enable SNe out to nearly 200 Mpc to be detected at mid-IR wavelengths, corresponding to a volume  $\sim 1000$  times larger than for *Spitzer*. So *MIRI* will be able to quickly observe large numbers of new SNe of all classes, both photometrically and spectroscopically, enabling the

dust contribution by each class to be accurately assessed.

I would like to thank Christoffel Waelkens and Xander Tielens for their comments and suggestions.

## References

1. Arnaboldi, M., et al.: *ApJ*, **472**, 145 (1996)
2. Barlow, M. J., et al.: *ApJ*, **627**, L113 (2005)
3. Benjamin, R. A., Churchwell, E. B., et al.: *PASP*, **115**, 953 (2003)
4. Bernard-Salas, J., Peeters, E., Sloan, G. C., Cami, J., Guiles, S., Houck, J. R.: *ApJ*, **652**, L29 (2006)
5. Bertoldi, F.; Carilli, C. L., Cox, P., Fan, X., Strauss, M. A., Beelen, A., Omont, A., Zylka, R.: *A&A*, **406**, L55 (2003)
6. Bouchet, P., Danziger, I. J.: *A&A*, **273**, 451 (1993)
7. Bowey, J. E., et al.: *MNRAS*, **331**, L1 (2002)
8. Bregman, J. N., Temi, P., Bregman, J. D.: *ApJ*, **647**, 265 (2006)
9. Carey, S. J.; Noriega-Crespo, A.; Price, S. D., et al.: *BAAS*, **207** 63.33 (2005)
10. Cernicharo, J., et al.: *A&A*, **315**, L201 (1996)
11. Cernicharo, J., Heras, A. M., Tielens, A. G. G. M., Pardo, J. R., Herpin, F., Gulin, M., Waters, L. B. F. M.: *ApJ*, **546**, L123 (2001)
12. Clayton, D. D., Amari, S., Zinner, E.: *Ap&SS*, **251**, 355 (1997)
13. Cohen, M., Barlow, M. J., Liu, X.-W., Jones, A. F.: *MNRAS*, **332**, 879 (2002)
14. Cox, P., et al.: *A&A*, **315**, L265 (1996)
15. Drew, J. E., et al.: *MNRAS*, **362**, 753 (2005)
16. Dunne, L., Eales, S., Ivison, R., Morgan, H., Edmunds, M.: *Nature*, **424**, 285 (2003)
17. Dwek, E., Galliano, F., Jones, A. P.: in 'A Century of Cosmology: Past, Present and Future', in press (2008), arXiv:0711.1170
18. Elvis, M., Marengo, M., Karovska, M.: *ApJ*, **567**, L107 (2002)
19. Gerardy, C. L., et al.: *ApJ*, **661**, 995 (2007)
20. Groenewegen, M. A. T., et al.: *MNRAS*, **376**, 313 (2007)
21. Grosdidier, Y., Moffat, A. F. J., Joncas, G., Acker, A.: *ApJ*, **506**, L127 (1998)
22. Iben, I. Jr., Renzini, A.: *ARAA*, **21**, 271 (1983)
23. Izumiura, H., Hashimoto, O., Kawara, K., Yamamura, I., Waters, L. B. F. M.: *A&A*, **315**, L221 (1996)
24. Jura, M., Morris, M.: *ApJ*, **251**, 181 (1981)
25. Kemper, F., Jaeger, C., Waters, L. B. F. M., Henning, Th., Molster, F. J., Barlow, M. J., Lim, T., de Koter, A.: *Nature*, **415**, 295 (2002)
26. Kotak, R., et al.: 2006, *ApJ*, **651**, L117 (2006)
27. Krause, O., Birkmann, S. M., Rieke, G. H., Lemke, D., Klaas, U., Hines, D. C., Gordon K. D.: *Nature*, **432**, 596
28. Lawrence, A., Warren, S. J., et al.: *MNRAS*, **379**, 1599 (2007)
29. Leonard, D. C., Filippenko, A. V., Barth, A. J., Matheson, T.: *ApJ*, **536**, 239 (2000)
30. Lucy, L. B., Danziger, I. J., Gouiffes, C., Bouchet, P.: in *IAU Colloq. 120, Structure and dynamics of the interstellar medium*, ed. G. Tenorio-Tagle, M. Moles, J. Melnick, Springer-Verlag, 164 (1989)
31. Markwick-Kemper, F., Gallagher, S. C., Hines, D. C., Bouwman, J., *ApJ*, **668**, L107 (2007)

32. Matsuura, M., Zijlstra, A. A., Molster, F. J., Waters, L. B. F. M., Nomura, H., Sahai, R., Hoare, M. G.: *MNRAS*, **359**, 383 (2005)
33. Meikle, W. P. S., et al.: *ApJ*, **665**, 608 (2007)
34. Meixner, M., et al.: *AJ*, **132**, 2268 (2006)
35. Méndez, R. H., et al.: *ApJ*, **491**, L23 (1997)
36. Molster, F. J., Lim, T. L., Sylvester, R. J., Waters, L. B. F. M., Barlow, M. J., Beintema, D. A., Cohen, M., Cox, P., Schmitt, B. L.: *A&A*, **372**, 165 (2001)
37. Morgan, H. L., Edmunds, M. G.: *MNRAS*, **343**, 427 (2003)
38. Morgan, H. L., Dunne, L., Eales, S. A., Ivison, R. J., Edmunds, M. G.: 2004, *ApJ*, **597**, L33 (2003)
39. Morris, P. W., et al.: *Nature*, **402**, 502 (1999)
40. Pozzo, M., Meikle, W. P. S., Fassia, A., Geballe, T., Lundqvist, P., Chugai, N. N., Sollerman, J.: *MNRAS*, **352**, 457 (2004)
41. Sloan, G. C., Kraemer, K. E., Matsuura, M., Wood, P. R., Price, S. D., Egan, M. P.: *ApJ*, **645**, 1118 (2006)
42. Smith, N., Foley, R. J., Filippenko, A. V.: *ApJ*, **680**, 568 (2008)
43. Sugerman, B. E. K., *ApJ*, **632**, L17 (2005)
44. Sugerman, B. E. K., et al.: *Science*, **313**, 196 (2006)
45. Sylvester, R. J., Kemper, F., Barlow, M. J., de Jong, T., Waters, L. B. F. M., Tielens, A. G. G. M., Omont, A.: *A&A*, **352**, 587 (1999)
46. Theuns, T., Warren, S. J.: *MNRAS*, **284**, L11 (1997)
47. Tielens, A. G. G. M., Waters, L. B. F. M., Bernatowicz, T. J.: in 'Chondrites and the Protoplanetary Disk', ASP Conference Series, vol. 341, 605 (2005)
48. Todini P., Ferrara A.: *MNRAS*, **325**, 726 (2001)
49. Tuthill, P. G., Monnier, J. D., Danchi, W. C.: in 'Interacting winds from massive stars', ASP Conf. Series, **260**, 321 (2002)
50. Tuthill, P., Monnier, J., Tanner, A., Figer, D., Ghez, A., Danchi, W.: *Science*, **313**, 935 (2006)
51. Waters, L. B. F. M., et al.: *Nature*, **391**, 868 (1998)
52. Weidemann, V.: *A&A*, **363**, 647 (2000)
53. Welch, D. L., Clayton, G. C., Campbell, A., Barlow, M. J., Sugerman, B. E. K., Meixner, M., Bank, S. H. R.: *ApJ*, **669**, 525 (2007)
54. Wooden, D. H., Rank, D. M., Bregman, J. D., Witteborn, F. C., Tielens, A. G. G. M., Cohen, M., Pinto, P. A., Axelrod, T. S.: *ApJS*, **88**, 477 (1993)